ACS OMEGA

http://pubs.acs.org/journal/acsodf

Article

Elucidating the Structural, Electronic, Elastic, and Optical Properties of Bulk and Monolayer MoS_2 Transition-Metal Dichalcogenides: A DFT Approach

Shehu Aminu Yamusa,* Amiruddin Shaari,* Norah A. M. Alsaif, Ibtihal M. Alsalamah, Ibrahim Isah, and Najeh Rekik*

Cite This: *ACS Omega* 2022, 7, 45719−45731

Read Online

ACCESS | Metrics & More | Article Recommendations

ABSTRACT: Due to their outstanding properties for optoelectronic and versatile electronic applications, the atomically thin layers of transition-metal dichalcogenide (TMDC) materials have demonstrated a potential candidacy to succeed its analog silicon-based technology. Hence, the elucidation of the most important features of these materials is indispensable. In this study, we provide a theoretical elucidation of the structural, electronic, elastic, and optical characteristics of TMDCs. The study has been carried out by elucidating the material in its two particular forms, namely, bulk and two-dimensional (2D) layered (monolayer). The theoretical investigation was carried out within the framework of the density functional theory (DFT) method using first-principles calculations. The Perdew−Burke−Ernzerhof (PBE) variant of the generalized gradient approximation (GGA) scheme, as performed in the Quantum Espresso package, is used. Van der Waals density functional effects, involving the nonlocal correlation part from the rVV10 and vdW-DF2 methods, were treated to remedy the lack of the long-range vdW interaction. An illustration of the performance of both rVV10 and vdW-DF2 functionalities, with the popular PBE correlations, is elucidated. The Born stability criterion is employed to assess structural stability. The obtained results reveal an excellent stability of both systems. Furthermore, the theoretical results show that band-gap energy is in excellent agreement with experimental and theoretical data. Pugh's rule suggested that both the bulk and MoS_2-2D layered systems are ductile materials. The refractive indices obtained herein are in good agreement with the available theoretical data. Moreover, the theoretical results obtained with the present approach demonstrate the ductility of both systems, namely, the bulk and the MoS_2-2D layered. The results obtained herein hold promise for structural, elastic, and optical properties and pave the way for potential applications in electronic and optoelectronic devices.

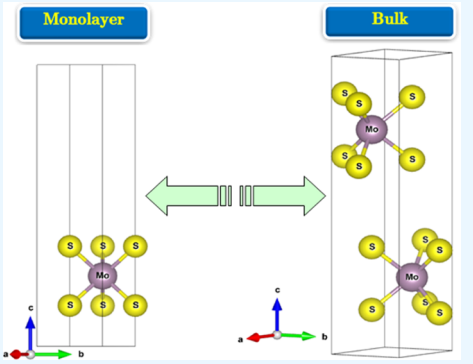

1. INTRODUCTION

Transition-metal dichalcogenide (TMDC) materials have recently gained a significant deal of attention in material research. In the last few decades, tremendous progress has been attained in the elaboration of high-quality atomically thin layers of TMDC materials. Moreover, TMDCs are a very promising type of semiconducting materials due to their attractive layer-dependent features, namely, the scalability and thickness-dependent optical and electrical features. Nowadays, these materials have demonstrated a potential candidacy to succeed their counterpart silicon-based technology. This achievement is predominantly due to their outstanding electrical, optical, sensing, and mechanical features for optoelectronic and versatile electronic applications.[1−5]

The field of transition-metal dichalcogenides has become a popular topic of research in condensed matter physics as well as a potential material for a variety of applications that have an impact on science and high-tech development. Researchers worldwide are particularly interested in the detailed response to its applications. Molybdenum disulfide (MoS_2) is considered one of the typical TMDCs. The exceptional properties of MoS_2 related essentially to the layer dependence of band structure as well as its specific direct band gap of 1.8 eV in monolayer make the material a promising remedy to gapless anomalies of graphene, thus making it an attractive material for a wide range of scientific and industrial research interests.[6] Molybdenum disulfide (MoS_2) is a unique semiconductor with a honeycomb structure that exhibits various mechanical, optical, and electrical properties, similar to graphene, making it the most desired material due to its

Received: November 1, 2022
Accepted: November 18, 2022
Published: November 29, 2022

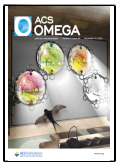

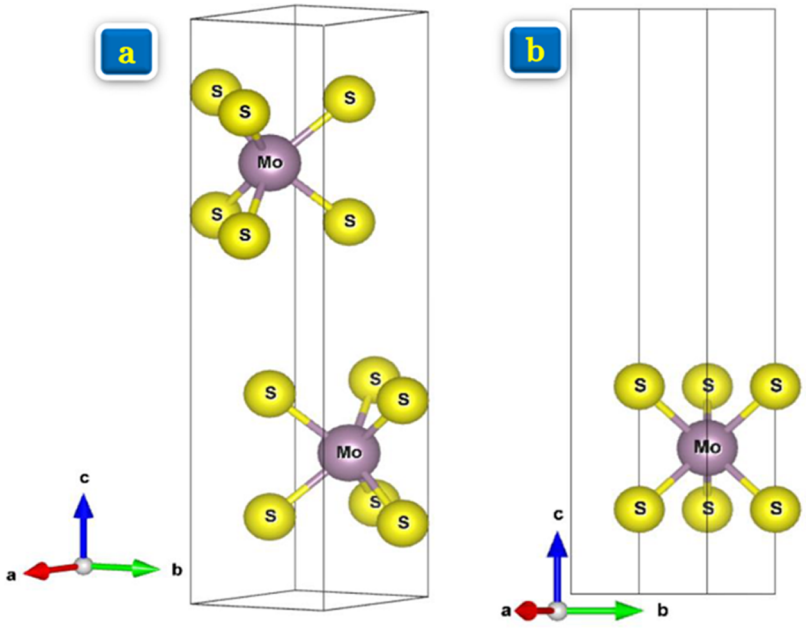

Figure 1. (a, b) Crystal structure of 2H-MX_2 (a) bulk and (b) monolayer.

wide range of industrial applications, beginning with lubricant, energy storage, photovoltaics, and catalysts.[7−10]

This material has a hexagonal crystal structure space group (*P*63/*mmc*). The MoS_2 bulk forms a layered semiconducting compound with the *P*3m1 space group.[11,12] The interlayer stacking of the compound possesses Mo metal atoms inserted between sulfur atoms having a nonmetal character with strong covalent bonds involved in the association of the sulfur metal. As shown in Figure 1, it is only mildly influenced by van der Waals forces.[13] Previous studies revealed that the material is a semiconductor with a narrow band gap.[11] However, considerable work remains to be done before the tools of electronic structure theory can be used by nonspecialists to engineer the properties of materials. The calculation of the mechanical stability, bulk modulus, and anisotropy of the system is much more important to unlock their potentiality.

Although many studies have been reported in the literature using different theoretical and experimental methods on MoS_2 for determining its corresponding electronic band-gap calculation, the experimental band gap for MoS_2 bulk and monolayer was reported with appropriate certitude by the pioneering work conducted by Mak et al.[14] The authors managed to reliably determine the band gap for MoS_2 bulk and monolayer to be 1.23 and 1.8 eV, respectively, which reveal that MoS_2 is a suitable material by both of its forms, namely, monolayer and bulk, for high-performance photodetector broad-band wavelengths. Cheng et al.[15] investigated the electronic and optical characteristics of the hexagonal structure of the MoS_2 crystal using DFT by employing the APW + lo method, which is very efficiently implemented in WIEN2k. Using this method, which considers the core and valence electrons to be self-consistent in a full-potential treatment, the authors reported the energy band gaps of 1.23 and 1.7 eV for MoS_2 bulk and monolayer, respectively. In another interesting work, Gyan et al.[16] studied MoS_2 energy band gaps by considering in their approach the plane-wave pseudopotential approximation within the LDA method and spin−orbit coupling within the generalized gradient approximation (GGA) method. The authors reported an indirect energy band gap in the range of 1.17−1.71 eV for bulk system and 1.6−1.71 eV for monolayer. Lahourpour et al.[17] reported a direct energy band gap of 1.50 eV at the K-point symmetry, determined within the (GGA) approach by employing the full-potential linear augmented plane waves and local orbital (FP-LAPW + lo) method. We should emphasize herein that even though the DFT approach is well adapted for the determination of the ground-state properties, band-gap energy calculated for MoS_2 bulk and monolayer is typically overestimated by the conventional techniques based on LDA or GGA.

In a subsequent study, Ahmad et al.[18] utilized the Quantum Espresso code's implementation of a self-consistent plane-wave pseudopotential total energy method (GGA-PW91). The outcome demonstrates that the estimated lattice parameters, a characteristic of typical GGA functional, overestimate the experimental values.[19] The results show that practically all structural values computed for bulk MoS_2 are equivalent to those calculated for monolayer MoS_2. The result also demonstrates that the bulk and monolayer bands are, respectively, 0.89 and 1.57 eV, which differ from the respective experimental values of 1.29 and 1.80.[20−22] To overwhelm this disagreement between the DFT simulations within LDA, GGA, and the experimental findings, the band-gap problem can be resolved more precisely by employing alternative approaches, such as the van der Waals interaction approximation, which provides a more accurate prediction of the fundamental band gap. In doing so, the optical and elastic properties were studied with different van der Waals density functionals to compare with the recent experimental and theoretical results. Due to quantum confinement, a direct-to-indirect band-gap transition from the monolayer form to the bulk one of MoS_2 results in a substantial increase in photoluminescence (PL), thereby enabling the opening of new horizons in the 2D material-based optoelectronic applications.

Numerous interesting features of the MoS_2 monolayer have been an active field of research in recent times.[23−26] In their study on the reflectance spectrum of bulk MoS_2, Beal and Hughes[27] observed that the maximum values of the real and

https://doi.org/10.1021/acsomega.2c07030
ACS Omega 2022, 7, 45719−45731

Table 1. Equilibrium Lattice Parameters, Volume, Bulk Modulus, and Their First-Derivative Modulus of Bulk and Monolayer MoS_2

phase	XC	a (Å)	c (Å)	V (Å^3)	B_0	B'
bulk MoS_2	PBE	3.18	12.38	109.49	131.1	3.96
	Rvv10	3.19	12.40	109.46	134.8	4.23
	vdW-DF2	3.23	12.56	119.46	111.5	4.65
	exp	3.17[a]	12.32[a]	107.18[a]		
		3.16[a]	12.29[a]			
	others	3.14[b]	12.43[b]	106.1[b]		
		3.18[c]				
monolayer MoS_2	PBE	3.18	12.38	108.67	66.4	4.49
	Rvv10	3.22	12.51	124.89	34.8	5.23
	VdW-DF2	3.25	12.65	116.42	57.7	4.55
	others	3.18[c]				
		3.195[b]				
	exp	3.16[a]	12.29[a]			

[a]Reference 33. [b]Reference 18. [c]Reference 12.

imaginary dielectric functions were 35 and 15, respectively. In a similar investigation, Hughes and Liang[28] determined for the particular direction E ∥ c within a vacuum experimental condition, the ultraviolet reflectivity spectra in a domain of energy ranging from 4.5 to 14 eV. Reshak and Auluck[29] have achieved comprehensive potential simulations of bulk MoS_2 for two different directions, namely, E ⊥ c and E ∥ c. However, we should underline that there is not much information or exhaustive studies dealing with the frequency-dependent optical features as well as electronic and mechanical features of the monolayer MoS_2 and bulk MoS_2 associated with the van der Waals effect.

As can be seen, the different theoretical methods proposed in the literature provide different conclusions, suggesting thereby that supplementary theoretical studies within the context of the density functional theory (DFT) with more deep approximations are disapprovingly crucial to elucidate the electronic, elastic, and optical properties of MoS_2 bulk and monolayers. Indeed, this elucidation will constitute a crucial first move for a force field for simulating the theoretical determination of the features of these new interesting materials. To the best of our knowledge, this work has not been completely accomplished. To do so, we present in this work a comprehensive study of the electronic, elastic, and optical properties of MoS_2 bulk and monolayers. This study is conducted within the framework of van der Waals density functional, as implemented by the Quantum Espresso and Thermo_pw packages using the density functional theory (DFT) method.

The structure of the present paper is as follows: Section 2 contains an overview of the detailed computational considerations employed herein. In Section 3, an illustration of the obtained theoretical results along with the physical discussions related to the elastic, structural, and optical properties of the materials studied herein is provided. Finally, concluding remarks are made in Section 4.

2. THEORETICAL CONSIDERATIONS

In the present study, all of the theoretical calculations considered herein for the ultimate objective of determining the structural, electronic, and optical properties of bulk and monolayered MoS_2 were performed by first-principles calculations based on DFT implemented by the Quantum Espresso package.[30] The high accuracy resulting from the effects of van der Waals density functionals, in turn, mainly results from the conjunction of the revised Vydrov−van Voorhis nonlocal correlation functional (rVV10), and the so-called vdW-DF2 method leads us to consider herein van der Waals density functionals by employing the PBE variant of the GGA method.[31,32] An excellent relaxation of the structure was achieved by considering a magnitude of the forces on each atom that is less than 0.01 eV/Å. A 12 × 12 × 3 and 12 × 12 × 1 Monkhorst−Pack mesh[29] is used to sample the Brillouin zone between Γ−K−M−Γ for the calculations of the structural and electronic properties of bulk and monolayer MoS_2, respectively. The Hartree exchange was evaluated by taking into consideration the correlation contribution to the total energy and Hamiltonian as well as a spacing of the real space grid having values of 400 Ry. The estimation of the optimized lattice parameters (a) and (c) used for the determination of the electronic, elastic, and optical features of bulk and monolayer MoS_2 is calculated using the parameters provided in Table 1. A 10-vacuum zone was created by dividing the monolayer MoS_2 along the c-axis. The thermo_pw quantum-ESPRESSO driver in conjunction with the QE package was used for the determination of the elastic and optical properties. The optical band parameters have been evaluated using an energy cutoff of 60 Ry in conjunction with 12 × 12 × 1 and 12 × 12 × 1 optical meshes for the bulk and monolayer MoS_2, respectively.

3. RESULTS AND DISCUSSION

3.1. Equilibrium Lattice Parameters. To determine the structural stability, we have calculated the total energy against the MoS_2 monolayer and the volume of MoS_2 bulk within PBE, rVV10, and vdW-DF2 density functionals. The obtained results are provided in Table 1 and compared with the available data. As can be depicted from the table, our results show that the two systems are more stable in a nonmagnetic state. This finding is in good agreement with the results reported by Ahmad et al.[34] Furthermore, the obtained equilibrium volume calculated within PBE and rVV10 functionals is in decent agreement with other experimental results,[31,35,36] whereas an excellent agreement is obtained with PAW-based calculations. The structural parameters were calculated for bulk MoS_2 and monolayer MoS_2. The obtained results are also provided in Table 1. The results obtained herein indicate that the inclusion of the van der Waals effect trains a systematic enhancement of

https://doi.org/10.1021/acsomega.2c07030
ACS Omega 2022, 7, 45719−45731

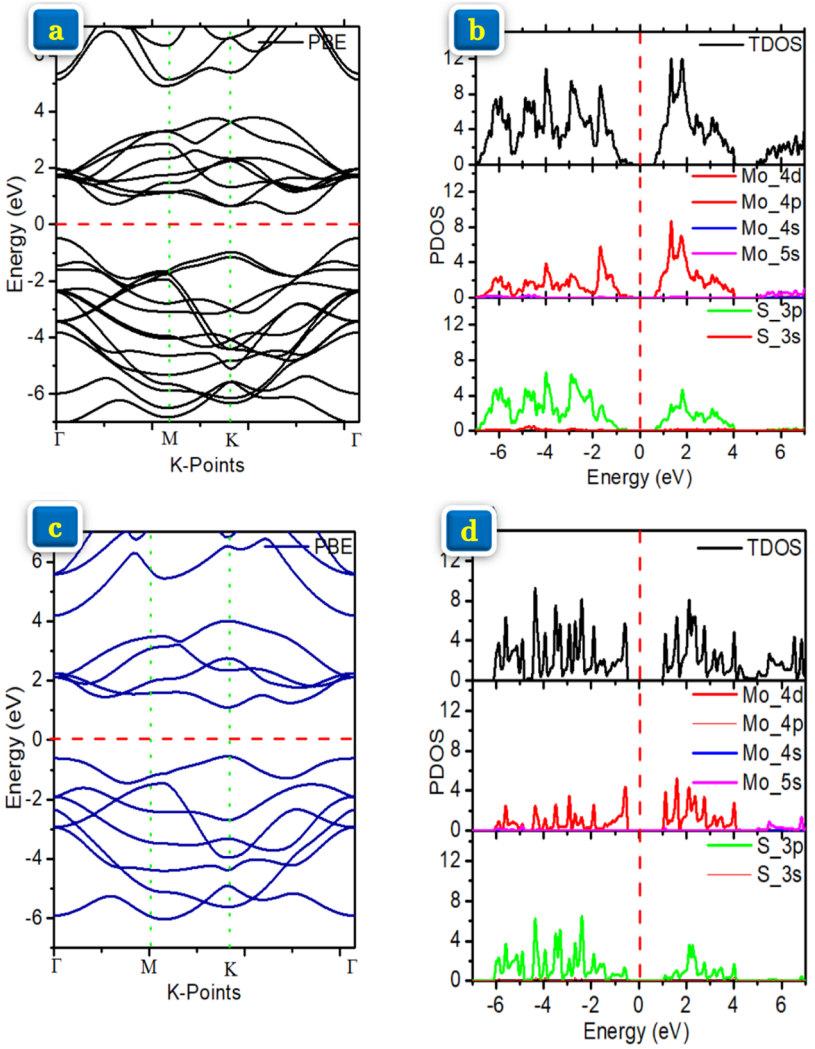

Figure 2. (a–d) Calculated band structure and density of state for (a) and (b) bulk MoS_2 within PBE and (c, d) monolayer within PBE.

the performance of the calculation, which significantly replicates the experimental findings.

3.2. Density of States and Electronic Band Structure. The bulk MoS_2 and the monolayer MoS_2 density of states and its corresponding electronic band structure, determined within the framework of the PBE, rVV10, and vdW-DF2 density functionals, and calculated in the first Brillouin zone at the high symmetry points Γ–K–M–Γ, are illustrated in Figures 2–5. The figures also show the total state density and the partial state density of the functionals. The band gap of the bulk MoS_2 corresponding to the energy separated between the conduction band (minima) and the valence band (maximum) that occurs between *K*–Γ and determined within the same density functionals, namely, PBE, rVV10, and vdW-DF2, takes the value of 0.84, 0.85, and 1.05 eV, respectively, as can be depicted in Table 1. Moreover, the results provided herein suggested that bulk MoS_2 is an indirect band-gap material. The obtained band gap is in excellent agreement with the results reported by Ataca et al.[37] These authors managed to reliably determine band gaps of 0.72 and 0.85 eV evaluated, respectively, by the use of the (LDA + PAW) and (GGA + PAW) pseudopotentials. We should emphasize herein that our calculated 1.05 eV band gap is similar to the value of 1.05 eV reported by Kumar et al.[38] using the (GGA + lo method). A band gap of 0.89 eV obtained using the rVV10 dispersion correction agrees with the result obtained by Ahmad et al.[18] who reported a value of 0.89 eV within GGA. For the monolayer MoS_2, the analysis of the position of the lowest point of the conduction band and the highest point of the valence band indicates a direct band-gap energy for this material. Our obtained energy gaps of 1.68, 1.62, and 1.55 eV evaluated within the use of PBE, rVV10, and vdW-DF2, respectively, show a pronounced effect of the vdW-DF2 functional.

Let us now discuss the density of bulk MoS_2 and monolayer states. These densities of states, which are specifically composed of four groups of states and bands in the occupied and unoccupied characterizing, respectively, the valence band maximum and the conduction band minimum states, are separated by the Fermi level at zero point energy. In the first group, the bands observed in the structure of the electronic band as well as the density of states ranging from −7 to −0.26 eV are primarily owing to the contribution of the 4d and 3p orbitals of the Mo and S atoms, respectively. The second group is located below the Fermi energy in the energy range from −0.26 to 0.49 eV, to which the 4d orbital of Mo and the 3p orbital of S are mostly contributing. In the third group located above the Fermi energy and for which the energy ranges

https://doi.org/10.1021/acsomega.2c07030
ACS Omega 2022, 7, 45719–45731

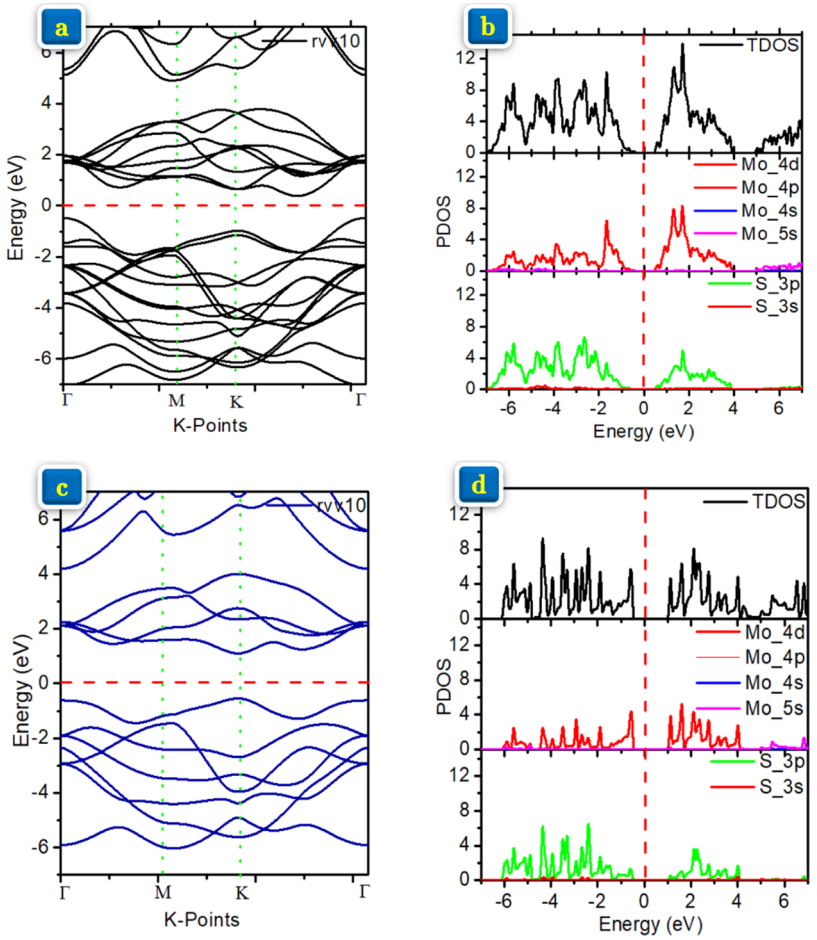

Figure 3. (a–d) Calculated band structure and density for (a) and (b) bulk MoS_2 within rVV10 and (c, d) monolayer within rVV10.

between 5.04 and 7 eV, the main contribution to the density of states and the electronic band structure is owing to the 4d orbitals of Mo and 3p orbitals of S, mainly contributing and showing strong hybridization. The fourth group located above 5.04 eV contributes to the lowest conduction bands, mostly from 5s and 3p of Mo and S orbitals. We should emphasize herein that on each side of the band gap, the observed bands are derived primarily from 3s of S and the 4d state of Mo in the MoS_2 bulk and the MoS_2 monolayer.[39,40] The bands located in the neighborhood of the band gap are quite flat. This is an encouraging result since this elucidation is primarily owing to the fact that the electron states at these energies possess a "d" character. Our results show that the reduction in the dimension of bulk MoS_2 to monolayer MoS_2 remains nonmagnetic (Table 2).

Compared to the previously published papers that are interesting,[42−44] the two structures of MoS_2 have been considered for the first time: the first one with the hole as no atom is present in the center of the hexagonal cage termed as 1H-MoS_2 and the second one with the presence of an atom at the center of the hexagonal cage termed as 1T-MoS_2. We started the calculation by employing generalized gradient approximation (GGA) and modified Becke−Johnson (mBJ) within a framework of density functional theory (DFT) with less computationally low-cost functional (van der Waals). Interestingly, both GGA and mBJ have given the same low value of band gaps. Therefore, a further calculation has proceeded with the computationally more expensive hybrid functionals like Heyd−Scuseria−Ernzerhof (HSE) and Becke−Lee−Yang−Par (BLYP) within the LCAO-DFT approach. The calculated value of band gap from HSE is found to be 2.35 eV, compared with the previously reported band gap from the GW method. However, the direct band gap calculated by the BLYP method is 1.83 eV, which is consistent with some of the experimental results. The presence of the direct band gap along the *K*−*K* symmetry in a UV−vis range predicts that 1H-MoS_2 is a potential candidate for optoelectronic applications.

3.3. Mechanical Properties. Many important solid-state properties are associated with elastic properties, such as the equation of states and Debye temperature. Elastic modulus and elastic constants provide a complete understanding of the elastic behavior of a crystalline solid such as the hardness, brittleness, stability of a material, ductility, and other mechanical constants.

3.4. Elastic Constant. The crystal's response to an externally imposed stress or strain is determined by its elastic stiffness, revealing thereby details regarding the structural stability, the bonding properties, and the mechanical stability. Generally, it is challenging to estimate the elastic constants from ab initio calculations because of the need to employ precise methods to determine the total stress complementary strain. For bulk, molybdenum sulfide exists in hexagonal space groups and has six elastic constants: five independent constants, namely, C_{11}, C_{12}, C_{13}, C_{33}, and C_{44} and the sixth one, namely, C_{66}, are determined by the following equation

https://doi.org/10.1021/acsomega.2c07030
ACS Omega 2022, 7, 45719−45731

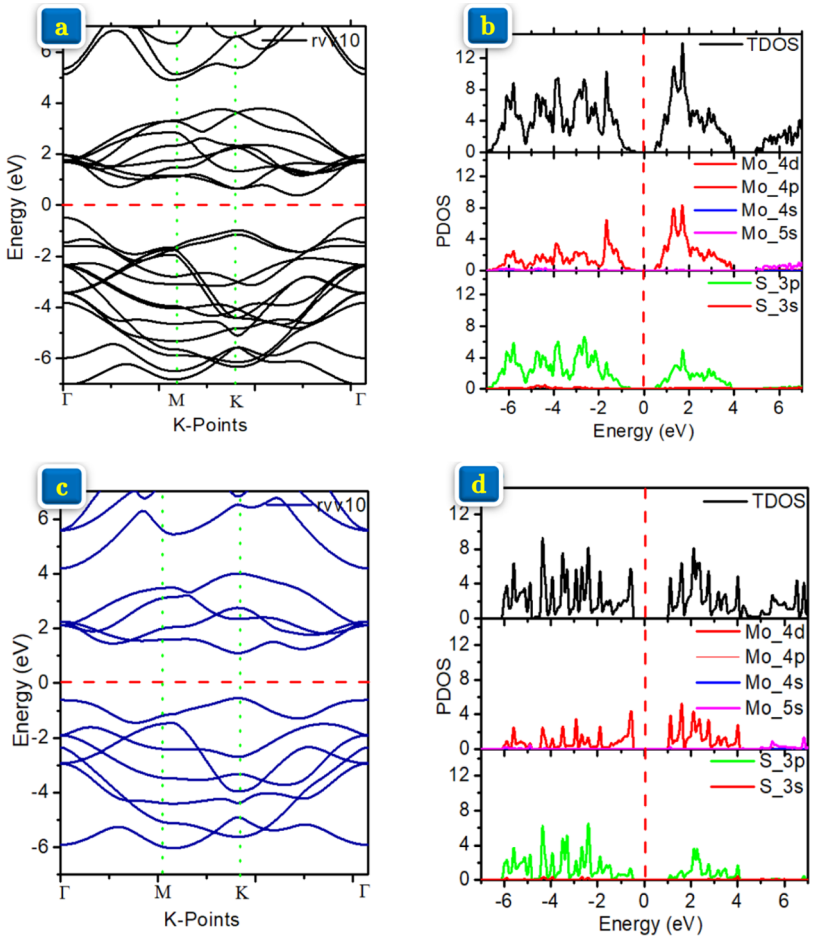

Figure 4. (a–d) Calculated band structure and density for (a) and (b) bulk MoS_2 within vdW-DF2 and (c, d) monolayer within vdW-DF2.

$$C_{66} = (C_{11} - C_{12})^2 \quad (1)$$

Generalized for monolayer, there are three independent elastic constants given by $\sigma_{ij} = C_{ij}\varepsilon_{ij}$: the first elastic constant is given by C_{11} and is due to σ_{11} to ε_{11}; likewise, for C_{22} and C_{12}, the values for C_{ij} are correlated to the equal volume of the MoS_2 unit cell.[45] Both the bulk and the monolayer were thoroughly tuned. The calculated elastic constants for both bulk and monolayer within the framework of PBE, rVV10, and vdW-DF2 functionals are reported in Table 3. These results are compared with the available theoretical and experimental measurements.[33,46] Under isotropic pressure, the mechanical stability of bulk and monolayer lattices must be carried out under the condition of Born criteria.[47] Mattheiss et al.[41] investigated the electronic structures and elastic properties of molybdenum disulfide using first-principles calculations. They reported an elastic constant (C_{ij}) of MoS_2 as a function of pressure that is ranging between 0 and 40 GPa. In another interesting work, Itas et al.[48] studied the hexagonal layered crystals' electronic and elastic properties using DFT+PBE +VdW. The authors reported that MoS_2 increased monotonically, and the increase in pressure trains an increase of the anisotropies. The macroscopic stability is always independent of the positive definiteness of the stiffness matrix.[49] The structural and elastic properties of MoS_2 are also studied in many interesting previous papers (for instance, see refs 50–52). The well-known Born stability criteria must satisfy a hexagonal structure with five independent elastic constants, as shown below

$$C_{11} \succ 0;\ \succ C_{33} \succ 0;\ C_{44} \succ 0 \quad (2)$$

$$(C_{11} - C_{12}) \succ 0 \quad (3)$$

$$(C_{11} + C_{12}) \succ C_{33} - 2 \times (C_{13})^2 \succ 0 \quad (4)$$

Table 3 demonstrates that both bulk and monolayer elastic constants are positive, indicating that the two systems are stable and that both the bulk and monolayer satisfy the Born mechanical stability limitation. As can be depicted in Table 3, our findings are in good accord with the measurements that have been reported in.[56,57] Furthermore, an improvement in the result presented herein compared to those reported by Yuan et al.[54] is elucidated. It can also be seen from Table 4 that C_{12}, C_{13}, C_{33}, and C_{44} increase within the use of PBE, rVV10, and vdW-DF2 functionals. Interestingly, the use of the vdW-DF2 functional favors obtaining a better result. Generally, our results show that the inclusion of the van der Waals interaction is susceptible to producing better results that are close to the experimental results. The small value C_{33}/C_{11} ratio and the big C_{13}/C_{12} ratio reveal that the atomic bonding along the *x*-direction is stronger than in the corresponding *z*-direction for both hexagonal atoms, indicating that the layered type with the layer perpendicular to the *c*-direction is correct.[58]

3.5. Elastic Modulus and Hardness. The mechanical properties of a hexagonal system can be computed using five

https://doi.org/10.1021/acsomega.2c07030
ACS Omega 2022, 7, 45719–45731

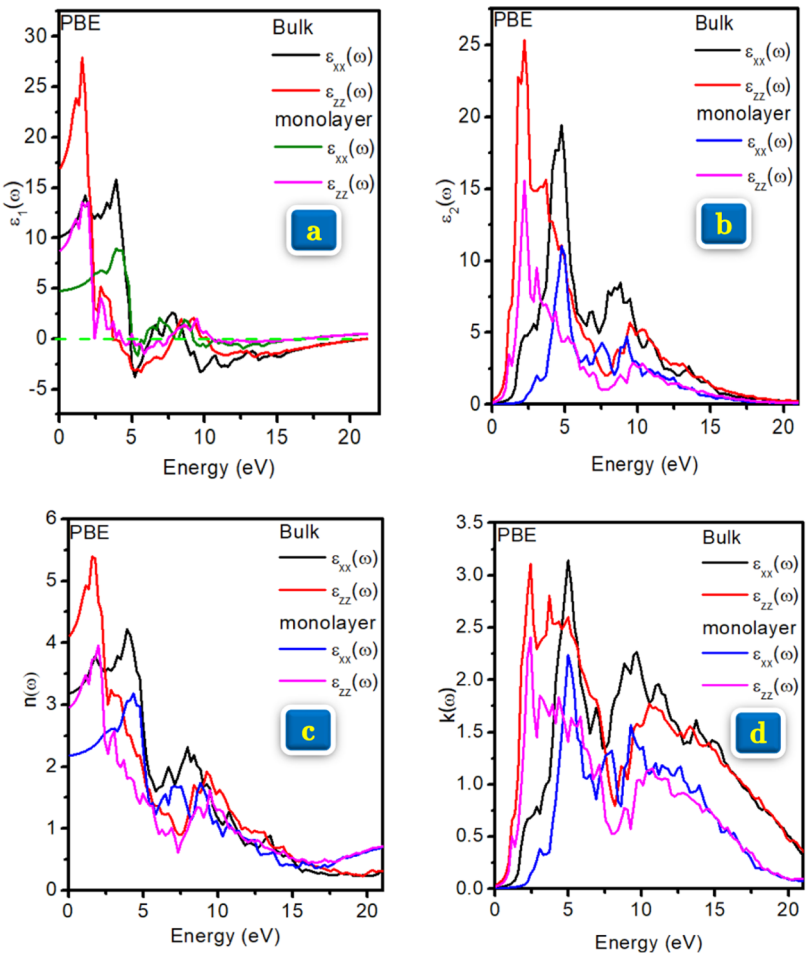

Figure 5. (a–d) Calculated real, imaginary, refractive index, and extinction coefficient of bulk and monolayer within PBE.

Table 2. Calculated Band Gap of Bulk and Monolayer of MoS_2

phase	PBE	PBE + rVV10	VdW-DF2	GGA	LDA + Lo	APW + Lo	GGA + Lo	others	exp
bulk MoS_2	0.86	0.89	1.05	0.89[18]	0.75[17]	1.23	1.05[17] 1.15[18]	1.90[35]	1.23[12]
monolayer MoS_2	1.68	1.62	1.55	1.57[34]	1.89[17]	1.7	1.55[17] 1.70[41]	1.78[31]	1.80[12]

Table 3. Elastic Constant of Bulk and Monolayer of MoS_2 within Different Functionals

bulk	PBE	rVV10	VdW-DF2	exp.[a]	others GGA[b]	others GGA[b]	monolayered	PBE	rVV10	VdW-DF2	others[c]	others[c]
C11	216.0	219.7	207.42	238	240.69	211	C11	112.50	99.82	94.82	149.42	130.4
C12	56.30	57.88	60.75	−54	53.64	49	C22	112.50	99.82	94.82	149.42	130.4
C13	11.20	16.63	20.49	23	8.5	3	C12	30.50	24.84	25.08	52.29	26.5
C33	38.30	63.33	68.87	52	56.11	37						
C44	26.50	31.12	28.17	19	26.10	30						

[a]Reference 53. [b]Reference 54. [c]Reference 55.

elastic constants C_{11}, C_{12}, C_{13}, C_{33}, and C_{44}. The machinability index, which determines the machinability of the system, can be obtained by dividing the bulk modulus B by the constant C_{44}. We should underline herein that usually higher the value of the ratio (B/C_{44}), the better the machinability. In this work, we have estimated the bulk modulus (B), the shear modulus (G), and Young's modulus (Y) for the individual C_{ij} for both bulk and monolayer structures to evaluate their effect on the physical quality of the materials. Pugh's rule suggested a parameter used to estimate whether the MoS_2 will be brittle or ductile. If the ratio (G/B) is superior to 0.57, then the material shown is ductile; else, it behaves as brittle.[53] In the present study, the calculated value of the ratio (G/B) of bulk and monolayer of MoS_2 shows a ductile nature of both forms. Du et al.[60] reported that the material properties can also be distinguished in terms of Poisson's ratio, suggesting that Poisson's ratio larger than 0.25 characterizes a ductile material; otherwise, it is a brittle material. In the study cases, Young's modulus is positive, which indicates that the atoms are compressed instead of being stretched.

https://doi.org/10.1021/acsomega.2c07030
ACS Omega 2022, 7, 45719−45731

Table 4. Calculated Bulk Modulus (B), Young's Modulus (E), Pugh's Ratio G/B, and the Poisson Ratio at Zero Pressure within Different Functionals

phase	XC	B (GPa)	E (GPa)	G (GPa)	A	n	G/B
bulk (MoS_2)	PBE	50.1	102.4	44.5	0.46	0.15	0.89
	rVV10	63.40	118.25	49.65	0.49	0.19	0.78
	VdW-DF2	65.56	111.51	45.84	0.48	0.21	0.69
	exp	47.65[a]					
		53.4					
	others	50.86[b]	107.38[b]	46.76[b]			1.09[b]
monolayer (MoS_2)	PBE	17.13	29.48	12.30	0.00	0.20	0.72
	rVV10	13.17	22.38	7.81	0.00	0.43	0.59
	VdW-DF2	9.05	25.19	9.99	0.00	0.26	1.10

[a]Reference 59. [b]Reference 54.

For the hexagonal structure of MoS_2, the bulk and the shear modulus can be deduced from the following equations

$$B_v = \frac{1}{9}[(2C_{11} + C_{12}) + C_{33} + 4C_{13}] \quad (5)$$

$$G_v = \frac{1}{30}(C_{11} + C_{12} - 2C_{33} + 4C_{13} + 12C_{44} + 12C_{66}) \quad (6)$$

Meanwhile, most of the experimental and synthesized systems are investigated in the form of ceramic polycrystalline; therefore, it is essential to determine the elastic parameters of the MoS_2 system in its polycrystalline state. To do so, we use herein the approximation of Voigt−Reuss−Hill, according to which two other important approximations are used, namely, the Voigt and Reuss approximations. The expressions of the shear and bulk moduli, provided in the pioneering Reuss model, are given by the following equations[55,61]

$$B_R = \frac{(C_{11} + C_{13})\,C_{33} - 2(C_{13})^2}{C_{11} + C_{12} + 2C_{33} - 4C_{13}} \quad (7)$$

$$G_R = \frac{5}{2}\frac{[(C_{11} + C_{12})\,C_{33} - 2(C_{13})^2]C_{44}C_{66}}{[3B_vC_{44}C_{66} + \{(C_{11} + C_{12})\,C_{33} - 2(C_{13})^2\}(C_{44} + C_{66})]} \quad (8)$$

The bulk modulus and the shear modulus, as approximated by Hill,[62] are used to calculate the effective modulus of anisotropic polycrystalline crystals, which is as follows

$$G = \frac{1}{2}(G_R + G_v) \quad (9)$$

$$B = \frac{1}{2}(B_R + B_v) \quad (10)$$

Then, the obtained bulk and shear moduli by Voigt−Reuss−Hill can be estimated by the average and the actual effective moduli, as seen in the following equation

$$E = \frac{9BG}{3B + G} \quad (11)$$

The polycrystalline species of MoS_2 obtained from B, G, and Y are represented by Poisson's ratio (ν), as shown in the following equation

$$\nu = \frac{3B - 2G}{2(3B + G)} \quad (12)$$

3.6. Anisotropy Factor. The study of elastic anisotropy in the design of crystals, especially layered materials, is important in science and engineering. The orientation dependency of the elastic moduli or sound velocities is known as crystal elastic anisotropy.[59,63] Because of its importance, a considerable effort has been made by researchers to provide a suitable elastic anisotropy index approach for layered materials, especially hexagonal structures. Zener and Siegel[64] measured cubic crystal anisotropy. However, this strategy only applies to cubic systems and cannot be applied to other systems; therefore, Itas et al.[65] (also see ref 66) suggested a scale for measuring the elastic anisotropy of a hexagonal system. Li et al.[67] studied the elastic anisotropy for 2D systems, and they found that, for hexagonal systems, the bounds are lattice-independent except for the highest symmetry lattice. In the present work, the anisotropy was calculated using eqs 13 and 14. As can be depicted in Table 3, only the bulk and monolayer shear anisotropic factors that can be estimated are presented. A equals 1 indicates an isotropic crystal, but any value less than 1 or more than 1 indicates anisotropy. The degree of the elastic anisotropy possessed by the crystal is usually indicated by deviation magnitude from the unity. Our calculated data provided in Table 4 show that the bulk of MoS_2 is anisotropy while the monolayer is zero, suggesting that it is isotropy by nature

$$\frac{k_c}{k_a} = \frac{(C_{11} + C_{12} + 2C_{13})}{C_{33} - C_{13}} \quad (13)$$

$$A_{an} = \frac{4C_{44}}{C_{44} + C_{44} + C_{44}} \quad (14)$$

$$A_{an} = \sqrt{\left(\frac{K^V}{K^R} - 1\right)^2 + 2\left(\frac{G^V}{G^R} - 1\right)^2} \quad (15)$$

The physical significance of A_{an} is the degree of distance between the normalized averaged stiffness tensor.

3.7. Optical Properties. The optical properties of the material clarify the material's behavior when exposed to electromagnetic radiation.[68] Light interaction with semiconductors must be well studied for optoelectronic technology applications. Electric vector **E** can be either perpendicular or parallel to the c-axis when calculating the dielectric characteristics of a compound with hexagonal symmetry. Using the Sternheimer approach, the complex dielectric constant of MoS_2 within the bounds of the independent particle approximation is determined. The proprietary branch of the Quantum Espresso project, Thermo_P.W. code,[69] applies the

https://doi.org/10.1021/acsomega.2c07030
ACS Omega 2022, 7, 45719−45731

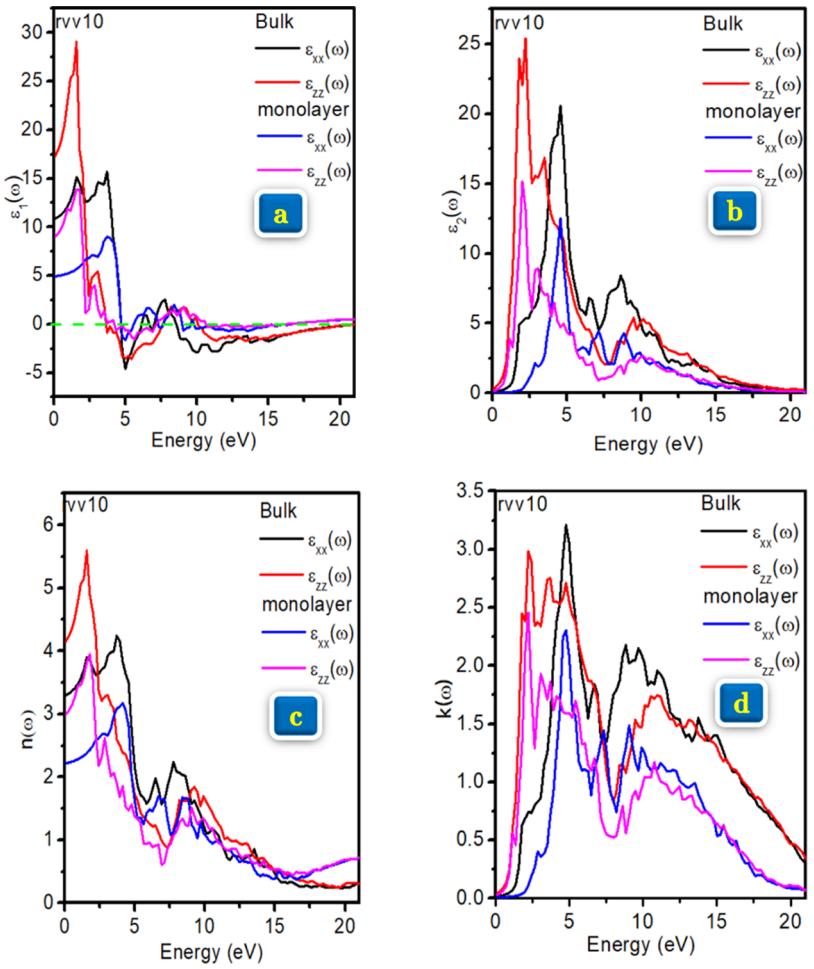

Figure 6. (a–d) Calculated real, imaginary, refractive index, and extinction coefficient of bulk and monolayer within rVV10.

Sternheimer method within time-dependent density functional theory (TDDFT).[4] One benefit of the Sternheimer technique is the ability to avoid computing the (many) empty states by introducing the projector to the empty states.[70] As a result, less time is spent idle on the CPU and RAM. The calculation will consume much CPU time across a wide frequency range.

The optical properties have been calculated in the energy range from 0 to 21 eV for both bulk and monolayer MoS_2. The calculated real and imaginary parts, refractive index, and extinction coefficient of the independent particle approximation are plotted in Figures 5a–d, 6a–d, and 7a–d, respectively. The amount of material polarization is typically determined by the real part of the macroscopic dielectric function. This polarization is primarily owing to the creation of electric dipoles generated by the external field. The static dielectric permittivity tensor $\varepsilon(0)$ principally describes the ionic contributions of a nonpolar system and enables the elucidation of the electronic contributions at high frequency. At high frequencies, the obtained dielectric constants $\varepsilon(\omega)$ have two contributions, namely, the interband $(\varepsilon_1(\omega))$ and intraband $(\varepsilon_2(\omega))$. The interband transition consists of direct and indirect transitions. We have shown in Figures 5–7 how the complex dielectric functions of the bulk and monolayer MoS_2, $\varepsilon_1(\omega)$ and $\varepsilon_2(\omega)$, varied with the energy (E) are entirely different. For the corresponding value ε_1 at $\omega = 0$, the magnitude of $\varepsilon_1(\omega)$ starts to increase with increasing the energy at the equilibrium position. The dielectric constant in the parallel and perpendicular directions evaluated with the three functionals is shown in Table 5 for both bulk and monolayer. Moreover, the values of $\varepsilon_2(\omega)$, evaluated with the three functionals, where the peaks occur and the corresponding photon energy values for the bulk and monolayer, are presented in Table 5.

The refractive index is a phenomenon that describes the bending of the incident light when it changes a medium. The refractive and extinction indices in parallel and perpendicular directions determined within the (DFT + PBE) approximations are similar to Yamusa et al.[71] These authors found the refractive index at zero frequency using a hexagonal structure for both bulk and monolayer. In the present work, a high index is observed for the studied material within the visible and infrared wavelength ranges and an index decreases at a higher energy in the UV region. The maximum peaks of the extinction coefficient for bulk and monolayer are shown in Table 5.

A variety of optical techniques, including absorbance, photoluminescence, and microreflectance spectroscopies, are now used to describe atomically thin TMDCs. However, spectroscopic ellipsometry (SE) is the best method for precisely determining the optical constant since it enables direct separation of the dielectric function across a large wavelength range from the raw data. SE has previously been used successfully to describe TMDCs. Although the data show a similar trend for a dielectric function (ε), its real (ε_1) and imaginary (ε_2) fundamental values can vary by up to 50%

https://doi.org/10.1021/acsomega.2c07030
ACS Omega 2022, 7, 45719−45731

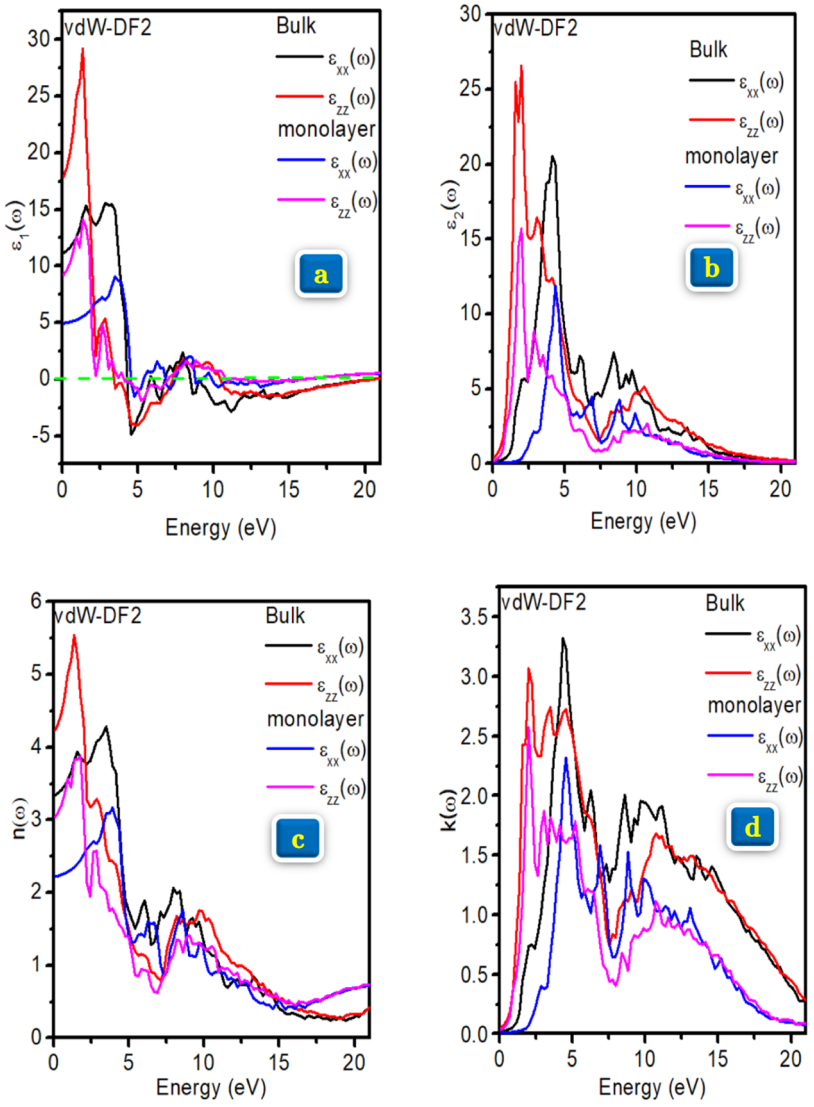

Figure 7. (a–d) Calculated real, imaginary, refractive index, and extinction coefficient of bulk and monolayer within vdW-DF2.

between various tests. These distinctions are brought about by optically energetic defects, the synthesis method, and the sensitivity of the physical properties of TMDCs to their dielectric surroundings. As a result, it is unclear which data should be used for the TMDC-based device model; therefore, to prevent errors, one must measure the optical constants for each sample. Therefore, the need for a reliable and repeatable method for determining the dielectric function of TMDCs is predominant. The growing interest in atomically thin layers of TMDCs and their potential uses and tasks, notably in sensing and optoelectronic devices, must be conveniently convoked by the expansion of theoretical tools. With the aid of such industrialists, researchers and tools may effectively link theoretical and experimental findings to create materials that are better suited for optoelectronic, sensing, and high-tech applications. The current study forms a part of such a method.

Remarkably, transition-metal dichalcogenide (TMDC) structures in bulk as well as monolayer exhibit an excitonic response; as result, substantial excitonic absorption is caused by the extreme refractive index in the near- and mid-infrared spectral intervals and the Kramers–Kronig relations. Furthermore, even at ambient temperature, excitons dominate optical absorption, photoluminescence, and spin-valley dynamics in TMDCs, enabling the development of room-temperature excitonic devices; i.e., as found in the current study, the real and imaginary components of the dielectric permittivity are ε_1 and ε_1, respectively, as shown in Figures 5 and 6. The electronic and optical properties of MoS_2 are also studied in many interesting previous papers (for instance, see refs 72–78).

4. CONCLUDING REMARKS

In this paper, we report a detailed computational description of structural, elastic, and optoelectronic characteristics of MoS_2 bulk and MoS_2-2D layered systems using DFT calculations. We performed numerical experiments using first-principles calculations for which the Perdew–Burke–Ernzerhof (PBE) variant of the generalized gradient approximation (GGA) scheme, as implemented in the Quantum Espresso package, is employed. Van der Waals density functional effects, involving the nonlocal correlation part from the rVV10 and vdW-DF2 methods, were also considered in this approach to remedy the lack of the long-range vdW interaction. Moreover, we employed the Born stability criteria to assess the structural stability. An elucidation of the performance of both rVV10 and

https://doi.org/10.1021/acsomega.2c07030
ACS Omega 2022, 7, 45719–45731

Table 5. Calculating the Real $\epsilon_1(\omega)$, Imaginary $\epsilon_2(\omega)$, Refractive Index $n(\omega)$, and Extinction Coefficient $k(\omega)$ of Bulk and Monolayer MoS_2 within Three Functionals (PBE, rVV10, and vdW-DF2)

system	functionals		$\epsilon_1(0)$	$\epsilon_2(\omega)$, eV	$n(\omega)$	$k(\omega)$
bulk	PBE	E ∥ c	10.02	2.19	3.18	3.11
		E ⊥ c	10.02	4.77	4.11	3.12
	rVV10	E ∥ c	10.85	2.19	3.29	3.22
		E ⊥ c	17.02	1.86	4.16	3.00
	vdW-DF2	E ∥ c	11.12	1.99	3.32	3.33
		E ⊥ c	17.68	1.59	4.22	3.08
	exp.			2.7[b]		
	others	E ∥ c	15.01[a]		3.88[a]	
		E ⊥ c	3.92[a]		2.96[a]	
monolayer	PBE	E ∥ c	4.77	2.18	2.18	2.25
		E ⊥ c	8.69	4.77	2.96	2.41
	rVV10	E ∥ c	4.88	2.67	2.21	2.31
		E ⊥ c	8.96	4.57	2.99	2.27
	vdW-DF2	E ∥ c	4.96	1.91	2.22	2.58
		E ⊥ c	9.18	4.39	3.02	2.33
	exp.					
	others	E ∥ c	4.92		2.15[a]	
		E ⊥ c	2.92		1.08[a]	

[a]Reference 6. [b]Reference 7.

vdW-DF2 functionalities with the popular PBE correlations was carried out. The results presented in this paper, dealing with MoS_2 bulk and MoS_2-2D layered systems using the above theoretical considerations, enable the pursuant conclusions and observations:

(i) The obtained results reveal excellent stability of both systems.
(ii) The theoretical results show that band-gap energy is in excellent agreement with experimental and theoretical data.
(iii) Pugh's rule suggested that both the bulk and MoS_2-2D layered are ductile materials.
(iv) The refractive indices obtained herein are in good agreement with the available theoretical data.
(v) The theoretical results performed with the present approach demonstrate the ductility of both systems.

Finally, it is crucial to note that the inclusion of the van der Waals interaction in the monolayer reveals a result that is closer to the experimental value than the bulk system. We are convinced that the enlargement of theoretical tools must conveniently convoy the growing interest in atomically thin layers of transition-metal dichalcogenides as well as their potential advantages and challenges, especially in sensing and optoelectronic devices. Using such tools, academics and industrialists will be able to associate both experimental results and theoretical findings in a viable way to conceive more suitable materials for optoelectronic, sensing, and high-tech applications. The present study constitutes a fragment of such a strategy.

AUTHOR INFORMATION

Corresponding Authors

Shehu Aminu Yamusa − *Department of Physics, Faculty of Science, Universiti Teknologi Malaysia, 81310 Johor Bahru, Malaysia; Department of Physics, Federal College of Education Zaria, 810282 Zaria, Kaduna State, Nigeria;* orcid.org/0000-0001-7948-1967; Email: aminuyamusa56@gmail.com, Shehu@graduate.utm.my

Amiruddin Shaari − *Department of Physics, Faculty of Science, Universiti Teknologi Malaysia, 81310 Johor Bahru, Malaysia*; Email: amiruddin@utm.my

Najeh Rekik − *Physics Department, Faculty of Science, University of Hail, Hail 55211, Saudi Arabia; Department of Chemistry, University of Alberta, Edmonton, Alberta T6G 2G2, Canada;* orcid.org/0000-0001-5347-1090; Email: rekik@ualberta.ca

Authors

Norah A. M. Alsaif − *Physics Department, College of Science, Princess Nourah Bint Abdulrahman University, Riyadh 11564, Saudi Arabia*

Ibtihal M. Alsalamah − *Physics Department, Faculty of Science, University of Hail, Hail 55211, Saudi Arabia*

Ibrahim Isah − *Department of Science and Laboratory Technology, Jigawa State Polytechnic, 720101 Dutse, Nigeria*

Complete contact information is available at: https://pubs.acs.org/10.1021/acsomega.2c07030

Notes

The authors declare no competing financial interest.

ACKNOWLEDGMENTS

The authors express their gratitude to Princess Nourah bint Abdulrahman University Researchers Supporting Project (Grant No. PNURSP2022R60) and Princess Nourah Bint Abdulrahman University, Riyadh, Saudi Arabia.

REFERENCES

(1) Itas, Y. S.; et al. Carbon nanotubes: A review of syntjesis and characterization methods/techniques. *Int. J. Sci. Technol.* **2020**, *8*, 43−50.

(2) Yang, S.-H.; Naaman, R.; Paltiel, Y.; et al. Chiral spintronics. *Nat. Rev. Phys.* **2021**, *3*, 328−343.

(3) Joon, H. C.; Kim, H. Quasiparticle band structures of bulk and few-layer $PdSe_2$ from first-principles GW calculations. cond-mat.mtrl-sci. *Phys. Rev.B* **2021**, *103*, No. 165419.

(4) Devgan, P. A review of Optoelectronic Oscillators for high-speed signal processing applications. *Int. Scholarly Res. Not.* **2013**, *16*, No. 401969.

(5) Žutić, I.; Fabian, J.; Sarma, S. D. Spintronics: Fundamentals and applications. *Rev. Mod. Phys.* **2004**, *76*, 323.

(6) Lawal, A.; Shaari, A.; Ahmed, R.; Taura, L. S.; Mohammad, L. M.; Idris, M. C. Sb_2Te_3/graphene heterostructure for broadband photodetector: A first-principles calculation at Cooper's exchange functionals level. *Optik* **2019**, *177*, 8392.

(7) Lopez-Sanchez, O.; Lembke, D.; Kayci, M.; et al. Ultrasensitive photodetectors based on monolayer MoS_2. *Nat. Nanotechnol.* **2013**, *8*, 497−501.

(8) Wu, M.; Jena, P. The rise of two-dimensional van der Waals ferroelectrics. *WIREs Comput. Mol. Sci.* **2018**, *8*, No. e1365.

(9) Lee, J.; Huang, J.; Sumpter, B. G.; Yoon, M. Strain-engineered optoelectronic properties of 2D transition metal dichalcogenide lateral heterostructures. *2D Mater.* **2017**, *4*, No. 021016.

(10) Yin, X.; Teng, A.; Chang, Z.; Yuan, P.; Zhang, D.; Yu, J. Investigations on Structural, Electronic and Optical Properties of MoS_2/CDs Heterostructure via First-Principles Study. *Catalysts* **2022**, *12*, 456.

(11) Gusakova, J.; Wang, X.; Shiau, L.; Krivosheeva, A.; Shaposhnikov, V.; Borisenko, V.; Gusakov, V.; Tay, B. Electronic Properties of Bulk and Monolayer TMDs: Theoretical Study Within

https://doi.org/10.1021/acsomega.2c07030
ACS Omega 2022, 7, 45719−45731

DFT Framework (GVJ-2e Method). *Phys. Status Solidi A* **2017**, *214*, No. 1700218.
(12) Hieu, N. N.; Ilyasov, V. V.; Vu, T. V.; Poklonski, N. A.; Phuc, H. V.; Phuong, L. T.; Hoi, B. D.; Nguyen, C. V. First principles study of optical properties of molybdenum disulfide: From bulk to monolayer. *Superlattices Microstruct.* **2018**, *115*, 10−18.
(13) Ermolaev, G. A.; Stebunov, Y. V.; Vyshnevyy, A. A.; et al. Broadband optical properties of monolayer and bulk MoS_2. *npj 2D Mater. Appl.* **2020**, *4*, 21.
(14) Mak, K. F.; Lee, C.; Hone, J.; Shan, J.; Heinz, T. F. Atomically thin MoS_2: a new direct-gap semiconductor. *Phys. Rev. Lett.* **2010**, *105*, No. 136805.
(15) Cheng, J.; Hu, P.; Ellis, P.; French, S.; Kelly, G.; Lok, C. M. Chain growth mechanism in Fischer- Tropsch synthesis: A DFT study of C-C coupling over Ru, Fe, Rh, and Re surfaces. *J. Phys. Chem. C* **2008**, *112*, 6082−6086.
(16) Gyan, M.; Botchway, F. E.; Parbey, J. Electronic Properties of Bulk and Single-Layer MoS_2 Using ab Initio DFT: Application of Spin-Orbit Coupling (SOC) Parameters. *East Eur. J. Phys.* **2020**, *4*, 69−74.
(17) Lahourpour, F.; Boochani, A.; Parhizgar, S. S.; Elahi, S. M.; et al. Structural, electronic and optical properties of graphene-like nano-layers MoX2(X:S,Se,Te): DFT study. *J. Theor. Appl. Phys.* **2019**, *13*, 191−201.
(18) Ahmad, S.; Mukherjee, S. A Comparative Study of Electronic Properties of Bulk MoS_2 and Its Monolayer Using DFT Technique: Application of Mechanical Strain on MoS2 Monolayer. *Graphene* **2014**, *03*, 52−59.
(19) Kube, C. M. Elastic anisotropy of crystals. *AIP Adv.* **2016**, *6*, No. 095209.
(20) Cline, C. F.; Dunegan, H. L.; Henderson, G. W. Elastic constants of hexagonal BeO, ZnS, and CdSe. *J. Appl. Phys.* **1967**, *38*, 1944−1948.
(21) Pan, Y.; Guan, W. Effect of sulfur concentration on structural, elastic and electronic properties of molybdenum sulfides from first-principles. *Int. J. Hydrogen Energy* **2016**, *41*, 11033−11041.
(22) Giannozzi, P.; Baroni, S.; Bonini, N.; et al. QUANTUM ESPRESSO: a modular and open-source software project for quantum simulations of materials. *J. Phys.: Condens. Matter* **2009**, *21*, No. 395502.
(23) Wiktor, J.; Ambrosio, F.; Pasquarello, A. Note: Assessment of the SCAN+ rVV10 functional for the structure of liquid water. *J. Chem. Phys.* **2017**, *147*, No. 216101.
(24) Granados del Águila, A.; Liu, S.; Do, T. T. H.; Lai, Z.; Tran, T. H.; Sean Ryan, K.; Zhi-Rui, G.; Zhang, H.; Yao, W.; Xiong, Q. Linearly Polarized Luminescence of Atomically Thin MoS2 Semiconductor Nanocrystals. *ACS Nano* **2019**, *13*, 13006−13014.
(25) Nguyen, A. D.; Pham, T. H.; Nguyen, T. K.; Ullah, H.; Tahir, Z.; Park, Y. C.; Park, J.; Jang, J. I.; Shin, Y. H.; Kim, Y. S. TiO_2 Nanorod Array Conformally Coated with a Monolayer MoS_2 Film: An Efficient Electrocatalyst for Hydrogen Evolution Reaction. *ACS Appl. Energy Mater.* **2020**, *3*, 10854−10862.
(26) Liu, S.; Granados del Águila, A.; Liu, X.; Zhu, Y.; Han, Y.; Chaturvedi, A.; Gong, P.; Yu, H.; Zhang, H.; Yao, W.; Xiong, Q. Room-Temperature Valley Polarization in Atomically Thin Semiconductors via Chalcogenide Alloying. *ACS Nano* **2020**, *14*, 9873−9883.
(27) Beal, A. R.; Hughes, H. Kramers-Kronig analysis of the reflectivity spectra of 2H-MoS_2, 2HMoSe_2, and 2H-MoTe_2. *J. Phys. C: Solid State Phys.* **1979**, *12*, 881.
(28) Beal, A. R.; Hughes, H. P.; Liang, H. The reflectivity spectra of some group V.A. transition metal dichalcogenides. *J. Phys. C: Solid State Phys.* **1975**, *8*, 4236.
(29) Reshak, A. H.; Auluck, S. Calculated optical properties of 2H-MoS_2 intercalated with lithium. *Phys. Rev. B* **2003**, *68*, No. 125101.
(30) Lee, K. Investigation of Exchange Energy Density Functional Accuracy for Interacting Molecules Related papers. *J. Chem. Theory Comput.* **2009**, *5*, 2754−2762.
(31) Perdew, J. P.; Burke, K.; Ernzerhof, M. Generalized gradient approximation made simple. *Phys. Rev. Lett.* **1996**, *77*, 3865.
(32) Hyldgaard, P.; Jiao, Y.; Shukla, V. Screening nature of the van der Waals density functional method: A review and analysis of the many-body physics foundation. *J. Phys.: Condens. Matter* **2020**, *32*, 393001.
(33) Wilson, J. A.; Yoffe, A. D. The transition metal dichalcogenides discussion and interpretation of the observed optical, electrical and structural properties. *Adv. Phys.* **1969**, *18*, 193−335.
(34) Ahmad, M.; Saeidi, P.; Yalameha, S.; Nourbakhsh, Z. First principles calculations of structural, electronic and optical properties MoX_2(X= S, Se) metal dichalcogenides and their nano-layers. *J. Magn. Magn. Mater.* **2020**, *503*, No. 166572.
(35) Wellendorff, J.; Lundgaard, K. T.; Møgelhøj, A.; Petzold, V.; Landis, D. D.; Nørskov, J. K.; Bligaard, T.; Jacobsen, K. W. Density functionals for surface science: Exchange-correlation model development with Bayesian error estimation. *Phys. Rev. B* **2012**, *85*, No. 235149.
(36) Klimeš, J.; Bowler, D. R.; Michaelides, A. Van der Waals density functionals applied to solids. *Phys. Rev. B* **2011**, *83*, No. 195131.
(37) Ataca, C.; Şahin, H.; Aktürk, E.; Ciraci, S. Mechanical and electronic properties of MoS_2 nanoribbons and their defects. *J. Phys. Chem. C* **2011**, *115*, 3934−3941.
(38) Kumar, A.; Ahluwalia, P. K. A first principle Comparative study of electronic and optical properties of 1H − MoS_2 and 2H − MoS_2. *Mater. Chem. Phys.* **2012**, *135*, 755−761.
(39) Dhanabalan, S. C.; Ponraj, J. S.; Zhang, H.; Bao, Q. Present perspectives of broadband photodetectors based on nanobelts, nanoribbons, nanosheets and the emerging 2D materials. *Nanoscale* **2016**, *8*, 6410−6434.
(40) Evanston, R. A.; Smirnov, V. Modification of the Monkhorst-Pack special points meshes in the Brillouin zone for density functional theory and Hartree-Fock calculations. *Phys. Rev. B* **2004**, *70*, No. 233101.
(41) Mattheiss, L. F. Energy Bands for 2H-$NbSe_2$ and 2H-MoS_2. *Phys. Rev. Lett.* **1973**, *30*, 784−787.
(42) Rai, D. P.; Vu, T. V.; Laref, A.; Hossain, M. A.; Haque, E.; Ahmad, S.; Khenata, R.; Thapa, R. Electronic properties and low lattice thermal conductivity of mono-layer (ML) MoS_2: FP-LAPW incorporated with spin−orbit coupling (SOC). *RSC Adv.* **2020**, *10*, 18830−18840.
(43) Rai, D. P.; Tuan, V. V.; Laref, A.; Ghimire, M. P.; Patra, P. K.; Srivastava, S. Electronic and optical properties of 2D monolayer (ML) MoS_2 with vacancy defect at S sites. *Nano-Struct. Nano-Objects* **2020**, *21*, No. 100404.
(44) Rai, D. P.; Vu, T. V.; Laref, A.; Joshi, H.; Patra, P. K. Promising optoelectronic response of 2D monolayer MoS_2: A first principles study. *Chem. Phys.* **2020**, *538*, No. 110824.
(45) Khatta, S.; et al. The first principles study of elastic and thermodynamic properties of ZnSe. *AIP Conf. Proc.* **2018**, *1953*, No. 130016.
(46) Gong, C.; Lee, G.; Shan, B.; Vogel, E. M.; Wallace, R. M.; Cho, K. First-principles study of metal-graphene interfaces. *J. Appl. Phys.* **2010**, *108*, 123711.
(47) Wu, Z.; Cohen, R. E. More accurate generalized gradient approximation for solids. *Phys. Rev. B* **2006**, *73*, No. 235116.
(48) Itas, Y. S.; Suleiman, A. B.; Ndikilar, C. E.; Lawal, A.; Razali, R.; Khandaker, M. U.; Ahmad, P.; Tamam, N.; Sulieman, A. The Exchange-Correlation Effects on the Electronic Bands of Hybrid Armchair Single-Walled Carbon Boron Nitride Nanostructure. *Crystals* **2022**, *12*, 394.
(49) Lebègue, S.; Eriksson, O. Electronic structure of two-dimensional crtals from ab initio theory. *Phys. Rev. B* **2009**, *79*, No. 115409.
(50) Wei, L.; Chen, J.; He, Q.; Wang, T. Electronic and elastic properties of MoS_2. *Physica B* **2010**, *405*, 2498−2502.
(51) Yue, Q.; Kang, J.; Shao, Z.; Zhang, X.; Chang, S.; Wang, G.; Qin, S.; Li, J. Mechanical and electronic properties of monolayer MoS_2 under elastic strain. *Phys. Lett. A* **2012**, *376*, 1166−1170.

https://doi.org/10.1021/acsomega.2c07030
ACS Omega 2022, 7, 45719−45731

(52) Cooper, R. C.; Lee, C.; Marianetti, C. A.; Xiaoding, W.; James, H.; Kysar, J. W. Nonlinear elastic behavior of two-dimensional molybdenum disulfide. *Phys. Rev. B* **2013**, *87*, No. 035423.
(53) Feldman, J. L. Elastic constants of 2H-MoS_2 and 2H-$NbSe_2$ extracted from measured dispersion curves and linear compressibilities. *J. Phys. Chem. Solids* **1976**, *37*, 1141−1144.
(54) Yuan, J. N.; Cheng, Y.; Zhang, X. Q.; et al. First-Principles Study of Electronic and Elastic Properties of Hexagonal Layered Crystal MoS2 Under Pressure. *Z. Naturforsch. A* **2015**, *70*, No. 529537.
(55) Plimpton, S. Fast Parallel Algorithms for Short-Range Molecular Dynamics. *J. Comput. Phys.* **1995**, *117*, 1−19.
(56) Nye, J. F.*Physical Properties of Crystals: Their Representation By Tensors and Matrices*; Oxford University Press, 1984.
(57) Akhter, M. J.; Kuś, W.; Mrozek, A.; Burczyński, T. Mechanical Properties of Monolayer MoS_2 with Randomly Distributed Defects. *Materials* **2020**, *13*, 1307.
(58) Wei, L.; Jun-fang, C.; He, Q.; Wang, T. Electronic and elastic properties of MoS_2. *Physica B* **2010**, *405*, 2498−2502.
(59) Chi, Z. H.; Zhao, X. M.; Zhang, H.; et al. Pressure-Induced Metallization of Molybdenum Disulfide. *Phys. Rev. Lett.* **2014**, *113*, No. 036802.
(60) Du, J.; Yu, H.; Liu, B.; Hong, M.; Liao, Q.; Zhang, Z.; Zhang, Y. Strain engineering in 2D material-based exible optoelectronics. *Small Methods* **2021**, *5*, No. 2000919.
(61) Ferlauto, A. S.; Ferreira, G. M.; Pearce, J. M.; Wronski, C. R.; Collins, R. W.; Deng, X.; Ganguly, G. Analytical model for the optical functions of amorphous semiconductors from the near-infrared to ultraviolet: Applications in thin film photovoltaics. *J. Appl. Phys.* **2002**, *92*, 2424−2436.
(62) Pan, Y.; Pu, D. Hydrogen embrittlement of C40 transition-metal disilicides. *J. Mater. Res.* **2019**, *34*, 3163−3172.
(63) Hill, R. The elastic behaviour of a crystalline aggregate. *Proc. Phys. Soc., Sect. A* **1952**, *65*, 349.
(64) Zener, C. M.; Siegel, S. Elasticity and Anelasticity of Metals. *J. Phys. Chem. A* **1949**, *53*, 1468.
(65) Itas, Y. S.; Suleiman, A. B.; Ndikilar, C. E.; et al. Computational Studies of the Excitonic and Optical Properties of Armchair SWCNT and SWBNNT for Optoelectronics Applications. *Crystals* **2022**, *12*, 870.
(66) Berkowitz, A.; Takano, K. Exchange anisotropy—a review. *J. Magn. Magn. Mater.* **1999**, *200*, 552−570.
(67) Li, R.; Shao, Q.; Gao, E.; Liu, Z. Elastic anisotropy measure for two-dimensional crystals. *Extreme Mech. Lett.* **2020**, *34*, No. 100615.
(68) Zhao, H.; Pettes, M. T.; Zheng, Y.; Htoon, H. Site-controlled telecom-wavelength single-photon emitters in atomically-thin $MoTe_2$. *Nat. Commun.* **2021**, *12*, No. 6753.
(69) Anju, S.; Mohanan, P. Biomedical applications of transition metal dichalcogenides (TMDCs). *Synth. Met.* **2021**, *271*, No. 116610.
(70) Peña, T.; Chowdhury, S. A.; Azizimanesh, A.; Sewaket, A.; Askari, H.; Wu, S. M. Strain engineering 2D MoS_2 with thin film stress capping layers. *2D Mater.* **2021**, *8*, No. 045001.
(71) Yamusa, S. A.; Shaari, A.; Isah, I. Structural stability, Electronic and Optical Properties of Bulk MoS_2 Transition Metal Dichalcogenides: A DFT Approach. *J. Appl. Phys.* **2022**, *14*, 40−44.
(72) Komsa, H.-P.; Krasheninnikov, A. V. Effects of confinement and environment on the electronic structure and exciton binding energy of MoS_2 from first principles. *Phys. Rev. B* **2012**, *86*, No. 241201.
(73) Molina'nchez, A.; Palummo, M.; Marini, A.; Wirtz, L. Temperature-dependent excitonic eects in the optical properties of single-layer. *Phys. Rev. B* **2016**, *93*, No. 155435.
(74) Liu, D.; Guo, Y.; Fang, L.; Robertson, J. Sulfur vacancies in monolayer MoS_2 and its electrical contact. *Appl. Phys. Lett.* **2013**, *103*, No. 183113.
(75) Kafi, F.; Shahri, R. P.; Benam, M. R.; Akhtar, A. Tuning Optical Properties of MoS_2 Bulk and Monolayer Under Compressive and Tensile Strain: A First-Principles Study. *J. Electron. Mater.* **2017**, *46*, 6158−6166.
(76) Dong, H. M.; Guo, S. D.; Duan, Y. F.; et al. Electronic and optical properties of single-layer MoS_2. *Front. Phys.* **2018**, *13*, No. 137307.
(77) Li, H.; Ji, A.; Zhu, C.; Cui, L.; Mao, L.-F. Layer-dependent bandgap and electrical engineering of molybdenum disulfide, Journal of Physics and Chemistry of Solids. *J. Phys. Chem. Solids* **2020**, *139*, No. 109331.
(78) Fan, X.; Chang, C.-H.; Zheng, W. T.; Kuo, J.-L.; Singh, D. J. The Electronic Properties of Single-Layer and Multilayer MoS under High Pressure. *J. Phys. Chem. C* **2015**, *119*, 10189−10196.

https://doi.org/10.1021/acsomega.2c07030
ACS Omega 2022, 7, 45719−45731